Inorganic Chemistry

Article

pubs.acs.org/IC

On the Road to MM′X Polymers: Redox Properties of Heterometallic Ni···Pt Paddlewheel Complexes

Marcello Gennari,[†,⊥] Gonzalo Givaja,[†] Oscar Castillo,[‡] Laura Hermosilla,[§] Carlos J. Gómez-García,[∥] Carole Duboc,[⊥] Agustí Lledós,[#] Ruben Mas-Ballesté,*[,†] and Felix Zamora*[,†]

[†]Departamento de Química Inorgánica, Universidad Autónoma de Madrid, 28049 Madrid, Spain

[‡]Departamento de Química Inorgánica, Universidad del País Vasco (UPV/EHU), Apartado 644, E-48080 Bilbao, Spain

[§]Departamento de Química Física Aplicada, Universidad Autónoma de Madrid, 28049 Madrid, Spain

[∥]Instituto de Ciencia Molecular (ICMol). Universidad de Valencia, Catedrático José Beltrán, 2, 46980 Paterna Valencia, Spain

[⊥]Univiversité Grenoble Alpes, CNRS, DCM, F-38000 Grenoble, France

[#]Departament de Química, Universitat Autònoma de Barcelona, 08193 Cerdanyola del Vallès, Spain

Supporting Information

ABSTRACT: On the quest of heterometallic mixed-valence MM′X chains, we have prepared two stable discrete bimetallic compounds: the reduced (PPN)[ClNi(μ-OSCPh)$_4$Pt] (PPN = bis(triphenylphosphine)iminium; OSCPh = benzothiocarboxylato) and the oxidized [(H$_2$O)Ni(μ-OSCPh)$_4$PtCl] species. The role of the aqua and chlorido axial ligands is crucial to facilitate oxidation of the {Ni(μ-OSCPh)$_4$Pt} core. Experimental and theoretical analyses indicate that a NiPt-Cl/Cl-NiPt isomerization process occurs in the oxidized species. The electronic structure of the reduced system shows two unpaired electrons, one located in a $d_{x^2-y^2}$ orbital of the Ni(II) ion and a second in the antibonding d_{z^2}−d_{z^2} combination from the Ni(II) and Pt(II) centers. Oxidation occurs by removing one electron from this second multicenter molecular orbital. Although the mixed-valence character of the oxidized species makes the isolation of MM′X chains very attractive, such polymeric structure is prevented by the low Pt−Cl···Ni interaction energy and the high tendency of Ni centers to coordinate water molecules. Thus, this work offers valuable insights and hints to engage the production of heterometallic mixed-valence MM′X chains, which still is a challenging task.

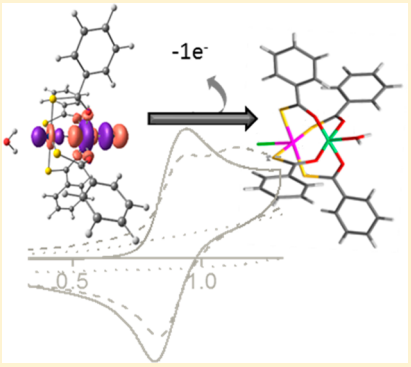

INTRODUCTION

The current boost in nanoscience favors the synthesis and characterization of forthcoming low-dimensional materials constructed by the combination of ligands and metal entities, so-called coordination polymers.[1] On demand technological applications require the development of molecular components with versatile electrical behavior across long distances. In this context, dimetal subunits (MM) have drawn attention in recent years due to their electronic properties[2,3] and their structural capabilities.[4] Heterodimetallic complexes can modulate electronic properties such as magnetism or electrical conductivity combining different metal ions.[5−7] Supramolecular polymerization of dimetal subunits allows the formation of a particular type of coordination polymers known as MMX-chains (X = bridging ligands between MM units). These coordination polymers have gained increased interest due to their outstanding magnetic and electrical properties at the bulk[8] and the nanoscale.[9] Among these, the family based on platinum and dithiocarboxylates subunits linked by iodine, $[Pt_2(RCS_2)_4I]_n$ (R = alkyl groups), shows unprecedented metallic conductivity at room temperature in the single crystal form.[10,11]Additionally, observations related to their chemical bond features have allowed researchers to process these materials both in solution[12,13] and by sublimation.[14] These unusual abilities have enabled the formation of sub-micro- and nanostructures. Thus, with the use of wet-lithography techniques, very stable and conductive sub-micrometer patterns have been produced.[12] Additionally, controlled sublimation of crystals of $[Pt_2(CH_3CS_2)_4I]_n$ allows the formation of well-defined highly conductive nanoribbons on mica[15] and SiO_2.[16] This breakthrough opens new perspectives for such materials in the field of molecular wires bypassing most common organic conductors.[17] Ruthenium MMX analogues have shown interesting magnetic properties[18,19] and the ability to be processed on surfaces.[20] More recently, $[Ru_2(RCO_2)_4X]_n$ (R = 3,4,5-tridodecyloxybenzoate, X = Cl or I) MMX-chains with dielectrophoretic capabilities under a given electrical field constitute prime examples of the renaissance of 1D metal−metal chains in the coordination nanomaterial chemistry realms.[21]

Received: July 11, 2014
Published: September 19, 2014

   dx.doi.org/10.1021/ic501659x | Inorg. Chem. 2014, 53, 10553−10562

The possibility to modulate the intrinsic electronic nature of selected MMX-chains and their basic building blocks, MM dimetal subunits, has been explored. This will enable the formation of new molecular wires with controlled electrical and/or magnetic properties. A rational way to get this specific goal comprises tuning the electronic properties of the bimetallic entity. In this context, the preparation of new heterobimetallic MM′X chains is certainly an interesting solution. Indeed, while mixed-metal MX-chains have been reported decades ago,[22] related MM′X compounds are limited to a few examples.[10,11,23−28] In particular, we have recently reported the first attempt to prepare heterobimetallic MM′X chains combining platinum with nickel or palladium containing dithiocarboxylato ligands.[7] The use of dithiocarboxylates as bridging ligands of the dimetal entities has led to formation of compounds with noncontrolled stoichiometries due to the scarce selectivity in the metal transmetalation reactions. Besides, this work has shown that the use of symmetric dithiocarboxylato ligands does not allow selective preparation of MM′ precursors for MM′X-chains. On the other hand, unsymmetrical monothiocarboxylato (R−C(S)O$^-$) ligands have been reported to form heterobimetallic entities in a controlled way, by direct reaction between the corresponding metal salts and the thiocarboxylic acids. However, up to this point, oxidation of heterobimetallic MM′ building blocks to yield mixed-valence species and their possible assemblies on 1D structures have not been achieved.

In this work, we have investigated the possibility to form novel MM′X-chains based on thiocarboxylato complexes of platinum and nickel via oxidation of MM′ dimetal entities [M = Pt(II), M′ = Ni(II)]. The electrochemical properties of these dimetallic complexes show that there are some intrinsic limitations in the oxidation process. In particular, we have isolated a [MM′−Cl]$^-$ precursor, which is more susceptible to oxidative processes than its neutral counterpart, MM′. Furthermore, we have carefully analyzed its oxidation capabilities and subsequent changes in electronic structure by DFT calculations. Finally, we discuss the factors governing intermolecular interactions in the mixed-valence oxidized [MM′−Cl] complex, which are crucial to form 1D structures.

RESULTS AND DISCUSSION

Synthesis of Reduced Cl−NiPt (1) and Oxidized NiPt−Cl (2) Species. Yellow crystals of the paddle-wheel complex (PPN)[ClNi(μ-OSCPh)$_4$Pt] (**1**) [PPN$^+$ = bis-(triphenylphosphoranylidene)ammonium, OSCPh = benzothiocarboxylato] were obtained from the previously reported [(H$_2$O)Ni(μ-OSCPh)$_4$Pt] species, by addition of 5 equiv of PPNCl in CH_2Cl_2 solution (Scheme 1). As expected, the chloride anion, like the H_2O molecule in the initial complex, is axially coordinated to the Ni(II) center, as attested by the X-ray structure of the product (*vide infra*). The presence of an excess of chloride is required to isolate **1**, to allow the complete substitution of the axial water molecule by a chloride anion. When a minor amount of chloride was employed (0.5 or 1 equiv vs initial complex), light green crystals of the initial water adduct [(H$_2$O)Ni(μ-OSCPh)$_4$Pt] were collected, thus providing evidence for the chemical reversibility of the substitution reaction. Coherently, when **1** is dissolved in CH_2Cl_2, the Ni-bound Cl$^-$ ion partially dissociates. Unfortunately, the UV−vis absorption and ^{1}H NMR properties of **1** are roughly identical to those of [(H$_2$O)Ni(μ-OSCPh)$_4$Pt]. However, the ESI-mass spectrum of a CH_2Cl_2 solution of [(H$_2$O)Ni(μ-OSCPh)$_4$Pt], in the presence of Bu$_4$NCl (from 0.5 to 5 equiv), shows a peak at m/z = 836.9, corresponding to the [ClNi(μ-OSCPh)$_4$Pt]$^-$ anion. In addition, a weak signal at m/z = 1637.9 (Supporting Information) can be attributed to a Cl$^-$-bridged [Pt(μ-OSCPh)$_4$Ni−Cl−Ni(μ-OSCPh)$_4$Pt] aggregate. This species is proposed to be present in solution when low Cl$^-$ amounts (1 equiv or less) are added (see below).

Scheme 1. Compounds Obtained in This Work

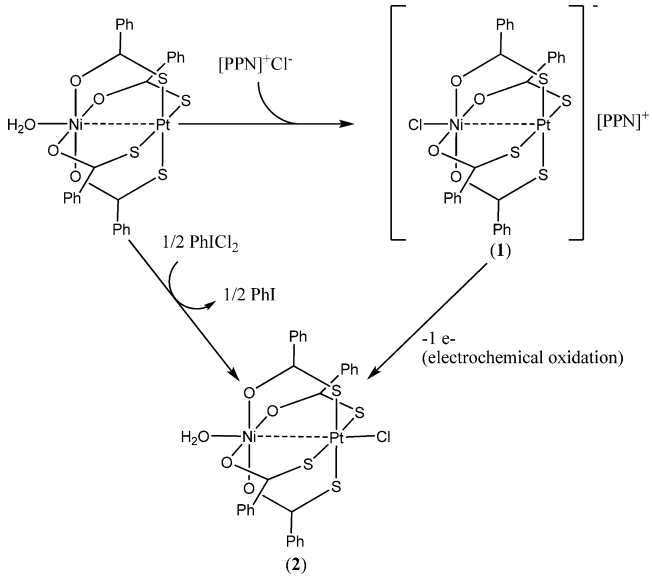

Concerning the synthesis of the mixed-valence [(H$_2$O)Ni(μ-OSCPh)$_4$PtCl] complex **2**, it can be obtained by chemical oxidation of [(H$_2$O)Ni(μ-OSCPh)$_4$Pt] with iodobenzene dichloride, which simultaneously acts as oxidizing agent and chlorido donor, in both THF or CH_2Cl_2. The same product can also be obtained by oxidation of [(H$_2$O)Ni(μ-OSCPh)$_4$Pt] with ammonium cerium(IV) nitrate in CH_2Cl_2:CH_3OH solution, in the presence of a source of chloride (Bu$_4$NCl, 1 equiv). Remarkably, in absence of chloride anions, the one-electron oxidation of [(H$_2$O)Ni(μ-OSCPh)$_4$Pt] by Ce(IV) does not occur. When bromide anions (Bu$_4$NBr, 1 equiv) are added instead of chloride, the formation of a transient oxidized product (very unstable even at −40 °C) was detected by UV−vis absorption spectroscopy. Finally, when using Bu$_4$NI (1 equiv), no oxidation occurs. All of these observations confirm the active role of chloride in promoting the oxidation of the bimetallic {Pt(μ-OSCPh)$_4$Ni} core, which is confirmed by cyclic voltammetry experiments (see below). The oxidized species **2** is paramagnetic, as confirmed by ^{1}H NMR and EPR spectroscopies, as well as by magnetic susceptibility measurements (see below). The X-ray structure of the product confirms the axial coordination of the chloride anion to the Pt center, whereas Cl$^-$ is bound to the Ni center in the corresponding reduced species (see below). The visible absorption spectrum of **2** (Figure 1) shows a band at 532 nm (ε = 830 M^{-1} cm^{-1}), while the optical spectrum of **1** is almost featureless in the visible region. Complex **2** is air stable in the solid state, although it slowly decomposes in solution (CH_2Cl_2, THF, ...). As shown by TGA, **2** is thermally stable up to 150 °C in solid state, meaning that the loss of the Ni-bound aqua ligand is not straightforward.

Structural Description of Reduced ClNiPt (1) and Oxidized NiPtCl (2) Species. Single crystal X-ray structural characterization reveals that compound **1** consists of paddle-

dx.doi.org/10.1021/ic501659x | Inorg. Chem. 2014, 53, 10553−10562

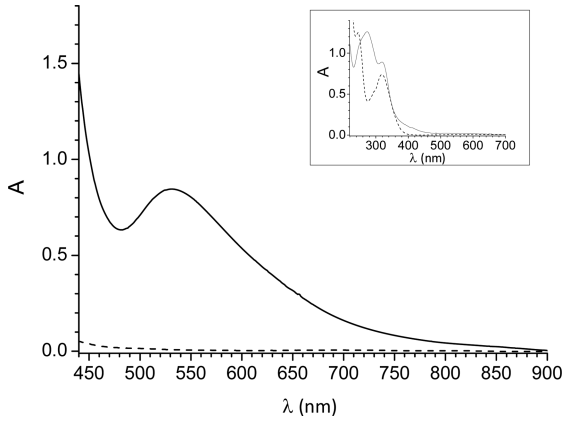

Figure 1. UV−vis absorption spectrum of **2** (—), compared to that of the initial product, $[(H_2O)Ni(\mu\text{-}OSCPh)_4Pt]$ (---) in CH_2Cl_2 under the same experimental conditions (1 mM solutions, 1 cm path length; inset: 0.1 mM, 2 mm path length).

wheel shaped $[ClNi(\mu\text{-}OSCPh)_4Pt]^-$ discrete entities, bis(triphenylphosphoranyl)iminium counterions, and disordered dichloromethane and water solvation molecules (Figure 2). Within the complex discrete entities, four thiobenzoato ligands bridge one platinum(II) and one nickel(II) metal centers into a heterometallic dimeric unit. The asymmetric thiocarboxylato group adopts a μ-κO:κS coordination mode in which the sulfur atom binds the platinum(II) ion and the oxygen atom to the nickel(II) ion, as expected from Pearson's HSAB concept. The Ni−O (2.05−2.07 Å) and Pt−S (2.32−2.33 Å) distances are in the range usually found in the bibliography. The Ni···Pt distance of 2.5940(7) Å is significantly shorter than the sum of van der Waals radii (r_{Ni}+r_{Pt} = 3.38 Å), indicative of the presence of a direct metal−metal interaction. The corresponding donor atom of the four thiocarboxilato ligands defines the equatorial plane of the coordination sphere of each metal, and the metal centers are slightly displaced outward from this plane, 0.026 and 0.009 Å for nickel and platinum, respectively. The NiO_4 and PtS_4 squares of the dimeric entity are rotated from the eclipsed arrangement by 19.18−19.99°. Nickel(II) shows a chloride anion anchored to the apical position at a distance of 2.325(2) Å, whereas platinum(II) is located 3.221(2) Å from a sulfur atom of an adjacent bimetallic entity. This weak Pt···S interaction arranges the heterometallic dimeric units into supramolecular dimeric aggregates.

Compound **2** is composed of neutral $[(H_2O)Ni(\mu\text{-}OSCPh)_4PtCl]$ entities and THF crystallization molecules (Figure 3). The structure of $[(H_2O)Ni(\mu\text{-}OSCPh)_4PtCl]$ dimeric entity closely resembles that of the analogous anionic dimer found in compound **1**, but with the particularity that oxidation implies a shortening of the Ni···Pt distance within the dimer from 2.5940(7) Å for compound **1** to 2.488(3) Å for compound **2**. This shortening implies that the displacement of the metal centers from the equatorial plane, although being small, now takes place inward the dimeric entity (0.026 and 0.019 Å for nickel and platinum, respectively). The rotation of the NiO_4 and PtS_4 squares from the eclipsed arrangement is lower than in compound **1** (12.45−15.75°). A careful comparison of the coordination bond distances (Table 1) for both dimers clearly shows an average shortening of the Ni−O bond distances, together with a lengthening of the Pt−S bonds when passing from **1** to **2**. The increase in the latter distances can be attributed to the presence of a strongly bonded chloride anion

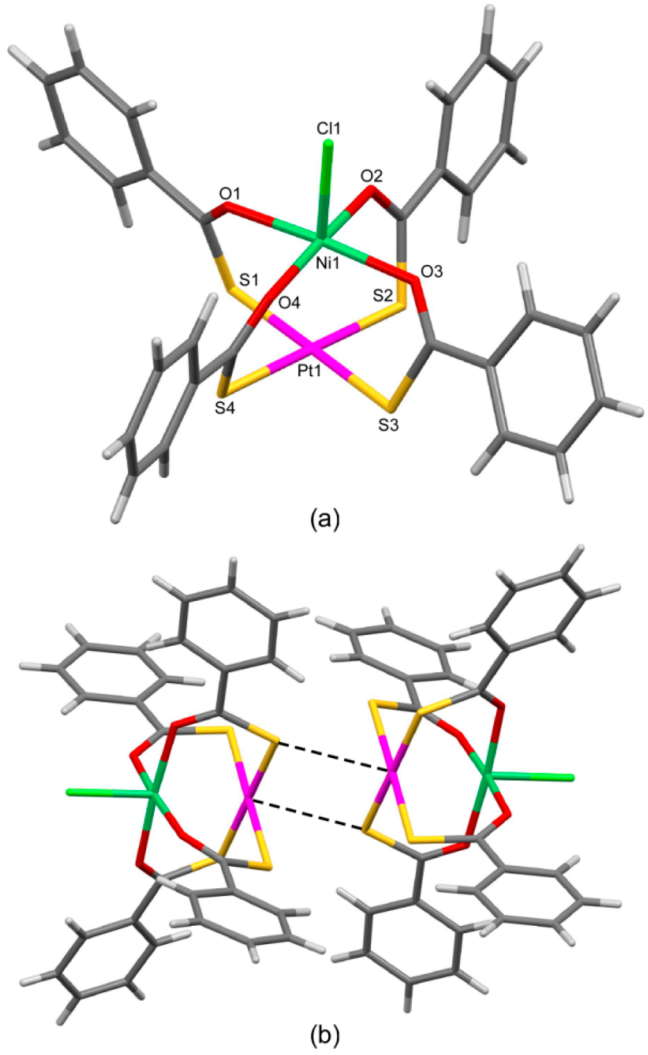

Figure 2. (a) View of the dimeric $[ClNi(\mu\text{-}OSCPh)_4Pt]^-$ entity found in compound **1** showing the labeling scheme. (b) Supramolecular assembly of two dimeric entities by means of weak Pt···S contacts.

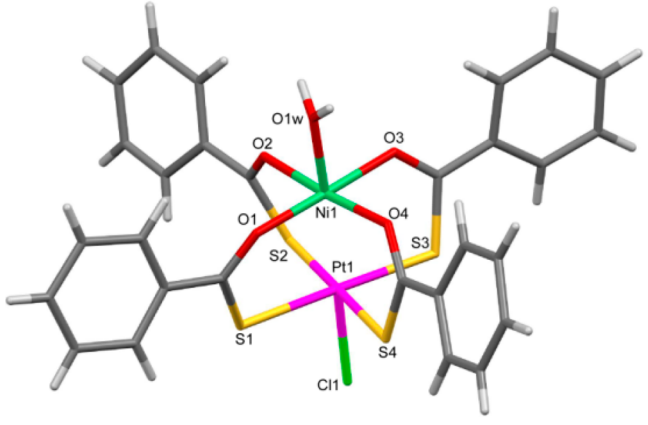

Figure 3. View of the $[(H_2O)Ni(\mu\text{-}OSCPh)_4PtCl]$ entity found in compound **2** showing the labeling scheme.

at the apical position of the platinum atom, which is not observed in the reduced species. This additional ligand results in an increase of the coordination number that usually implies a lengthening of the coordination bond distances. The supramolecular crystal building is established by a cooperative

dx.doi.org/10.1021/ic501659x | *Inorg. Chem.* 2014, 53, 10553−10562

Table 1. Comparison between the Bond Distances (Å) in the Coordination Sphere of Pt and Ni in Compounds 1 and 2, Obtained from X-ray Diffraction

	1	2		1	2
Ni–O1	2.049(4)	1.999(17)	Pt–S1	2.328(2)	2.355(7)
Ni–O2	2.063(4)	2.080(15)	Pt–S2	2.319(2)	2.354(6)
Ni–O3	2.058(4)	2.017(18)	Pt–S3	2.323(2)	2.368(7)
Ni–O4	2.066(4)	2.011(16)	Pt–S4	2.320(2)	2.357(6)
Ni–X_{axial} [a]	2.3252(15)	1.999(17)	Pt–X_{axial} [b]		2.430(5)
Ni···Pt	2.5940(7)	2.488(3)			

[a] X_{axial}: Cl1 for **1** and O1w for **2**. [b] X_{axial}: Cl1 for **2**.

assembly of hydrogen bonding interactions (O–H···O, C–H···Cl) and some additional van der Waals interactions involving the aromatic ring of the benzene molecule.

EPR Characterization of Oxidized NiPtCl (2) Species. To our knowledge, no EPR studies on mixed-valence discrete heterobimetallic MM′X paddle-wheel complexes have been reported in the literature until now. In fact, the closest example found in literature consists of the EPR investigation on quasi-one-dimensional homometallic PtPtI complexes.[11,23]

The powder X-band EPR spectrum of **2** displays a slightly rhombic $S = {}^1/_2$ signal (Figure 4a), with $g_x = 2.075$, $g_y = 2.105$, and $g_z = 2.335$. In order to better reproduce the experimental data, hyperfine coupling interaction related to ^{195}Pt (33.8% abundance, $I = {}^1/_2$) has been added with $A_x{}^{195}\text{Pt} = 550$ MHz. In CH_2Cl_2 solution (Figure 4b), the spectrum becomes axial, with $g_\perp = 2.062$ and $g_\parallel = 2.312$: the loss of rhombicity is consistent with a slight structural change of **2** in solution with respect to the solid state. Nevertheless, the fact that both EPR spectra are comparable with $g_\parallel > g_\perp > 2.0023$ in solution and $g_z > g_y \simeq g_x > 2.0023$ in powder attests to the paddle-wheel structure of **2** being retained in solution.

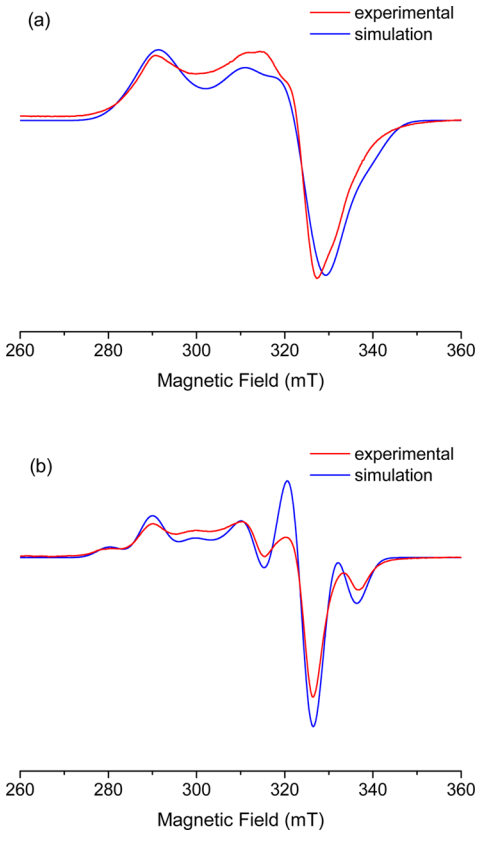

Figure 4. Experimental (red line) and simulated (blue line) X-band EPR spectra of **2** in solid state (a) and in CH_2Cl_2 solution (1 mM, b), at 100 K.

In a CH_2Cl_2 solution of **2**, the observation that $g_\parallel > g_\perp > 2.0023$ shows that the unpaired electron is mainly localized over the Ni d_{x2-y2} orbital, in agreement with the composition of the singly occupied molecular orbital (SOMO) of **2** (see below). However, the hyperfine couplings related to the Pt are surprisingly large with $A_\parallel{}^{195}\text{Pt} = 610$ MHz, $A_\perp{}^{195}\text{Pt} = 585$ MHz. This suggests a significant degree of delocalization of the unpaired electron onto the Pt center, which is apparently incompatible with the Ni character of the SOMO orbital. However, as attested by the calculated atomic spin densities of **2**, some unpaired electron density (0.28) is present in the platinum center and 0.4 electrons for the LUMO (see below); some unpaired electron density is present also in the HOMO and LUMO, which have a high contribution of the platinum.

Magnetic Characterization of Reduced ClNi-Pt (1) and Oxidized NiPt-Cl (2) Species. The thermal variation of the $\chi_m T$ product (χ_m is the molar magnetic susceptibility per NiPt dimer) for compound **1** shows a room temperature value of *ca.* 1.10 cm^3 K mol^{-1}, corresponding to the presence of two unpaired electrons (with a g value close to 2.1). When the temperature is decreased, $\chi_m T$ remains constant down to *ca.* 50 K. At lower temperatures, it shows a progressive decrease to reach a value of *ca.* 0.20 cm^3 K mol^{-1} at 2 K (Figure 5). This behavior agrees with the presence in compound **1** of two unpaired electrons with a very weak antiferromagnetic intermolecular coupling and/or a zero field splitting (ZFS) of the $S = 1$ spin ground state. The thermal variation of χ_m shows a rounded maximum appearing at *ca.* 2.3 K (inset in Figure 5), suggesting the presence of a weak, although not negligible, antiferromagnetic coupling. However, in order to check all the possibilities, we have used the three, *a priori*, more plausible models: (i) an isolated $S = 1$ NiPt unit with ZFS, (ii) a coupled dimer model constituted by two $S = 1$ NiPt units with no ZFS, and (iii) as in model ii but including a ZFS.[29,30] Model i reproduces satisfactorily the magnetic properties of **1** (black line in Figure 5) with $g = 2.098$ and $|D| = 19.7$ cm^{-1} (note that from powder magnetic susceptibility measurements we cannot determine the sign of D). Model ii gives a very good fit, but only in the high temperature range (red line in Figure 5) with $g = 2.138$ and $J = -3.7$ cm^{-1} (the Hamiltonian is written as $H = -JS_1S_2$). Finally, model iii gives a much better agreement with

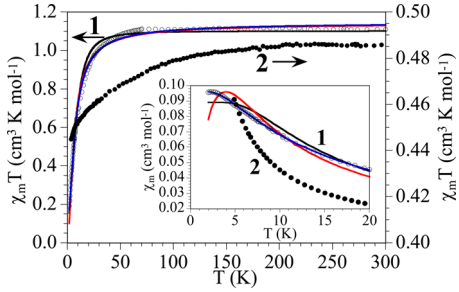

Figure 5. Thermal variation of $\chi_m T$ for compounds **1** (left scale) and **2** (right scale). Solid lines are the best fit to the isolated $S = 1$ dimer model with ZFS (black line), $S = 1$ interacting dimers model (red line), and $S = 1$ interacting dimers model with ZFS (blue line). Inset shows the low temperature region of the thermal variation of χ_m.

dx.doi.org/10.1021/ic501659x | Inorg. Chem. 2014, 53, 10553–10562

the experimental data in the whole temperature range, including the rounded maximum at *ca.* 2 K in the χ_m versus T plot, with g = 2.142, $|D|$ = 13.7(3) cm^{-1}, and J = −1.9(1) cm^{-1} (blue line in Figure 5). The D value in model iii is much more realistic than that found in model i, and therefore, we can assume that compound **1** presents both effects: a weak interdimer antiferromagnetic coupling and the ZFS of the S = 1 spin ground state. The weak antiferromagnetic coupling between the PtNi units probably is due to the presence of two semicoordinative Pt···S bonds that link the PtNi units into dimers (see structural description). This weak coupling (through two semicoordinative Pt···S···Pt bridges) contrasts with the much stronger one (J = −60 cm^{-1}) found in the related $[(H_2O)Ni(\mu\text{-}OSCPh)_4Pt]$ complex where direct Pt···Pt interactions (of *ca.* 3.08 Å) are claimed to be responsible for this strong coupling.[6]

The thermal variation of $\chi_m T$ for the oxidized compound **2** per PtNi dimer shows a room temperature value of *ca.* 0.48 cm^3 K mol^{-1}, much lower than the one observed for the reduced derivative **1**. On cooling the sample, the $\chi_m T$ value decreases very slowly and reaches a value of *ca.* 0.45 cm^3 K mol^{-1} at 2 K (Figure 5). This behavior indicates that compound **2** contains one unpaired electron ($S = {}^1/_2$).

These results fully agree with theoretical calculations (*vide infra*) that suggest that the reduced compound **1** presents two unpaired electrons, while the oxidized compound **2** has only one unpaired electron.

Electrochemical Behavior of Reduced Bimetallic Species. The redox properties of $[(H_2O)Ni(\mu\text{-}OSCPh)_4Pt]$, in the absence and presence of chloride anions, and those of the corresponding oxidized product, **2**, have been studied by cyclic voltammetry (CV) in CH_2Cl_2 solution. In the CV of $[(H_2O)Ni(\mu\text{-}OSCPh)_4Pt]$ (ESI) a poorly defined highly irreversible oxidation peak is located at Ep_a = +1.72 V. This multielectron process can be tentatively assigned to a ligand-based oxidation. A much more intense reversible reduction peak is located at Ep_c = −1.55 V: this signal can be attributed to solvent reduction, catalyzed by a reduced form of the complex. Whereas the reduction process is essentially not affected by the presence of chloride ions in solution, the oxidation properties of the paddle-wheel complex $[(H_2O)Ni(\mu\text{-}OSCPh)_4Pt]$ are completely modified when tetrabutylammonium chloride is added to the complex (Figure 6a). When up to 1 equiv of Bu_4NCl is added, two oxidation peaks appear, a reversible one located at $E_{1/2}$ = +0.88 V (ΔEp = 120 mV, Ep_a = +0.94 V, Ep_c = +0.82 V) and one irreversible located at Ep_a = +1.13 V. The first system can be assigned to the one-electron oxidation of the $[ClNi(\mu\text{-}OSCPh)_4Pt]^-$ species. Notably, a very low geometrical reorganization of the paddle-wheel structure after oxidation must be envisaged, in order to explain the electrochemical reversibility of the redox process. This implies the formation of a $[ClNi(\mu\text{-}OSCPh)_4Pt]$ oxidized species with the Cl^- anion coordinated to Ni, like in the corresponding reduced species. Concerning the attribution of the second redox system, it is worth mentioning that, when up to 1 equiv of chloride is present in solution, the species $[ClNi(\mu\text{-}OSCPh)_4Pt]^-$ is in equilibrium with the initial complex $[Pt(\mu\text{-}PhCOS)_4Ni(H_2O)]$ and also with a Cl-bridged species, $[Pt(\mu\text{-}OSCPh)_4Ni{-}Cl{-}Ni(\mu\text{-}OSCPh)_4]^-$ (see before), that can be detected by ESI-MS (peak at m/z = 1637.9). Thus, the second redox system can be attributed to the one-electron oxidation of the latter bridged species into the corresponding $[Pt(\mu\text{-}OSCPh)_4Ni{-}Cl{-}Ni(\mu\text{-}OSCPh)_4]$ complex, followed by an asymmetric dissociation

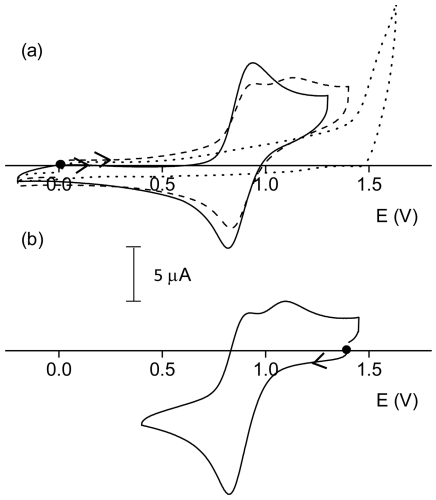

Figure 6. Cyclic voltammograms of (a) a 1.0 mM solution of $[(H_2O)Ni(\mu\text{-}OSCPh)_4Pt]$, before (···) and after addition of 1 equiv (---) and 1.5 equiv (—) of Bu_4NCl, and of (b) a 1.0 mM solution of **2**, both in CH_2Cl_2 0.1 M Bu_4NPF_6 (carbon vitreous electrode, scan rate of 100 mVs^{-1}, potentials vs Ag/AgCl).

yielding $[ClNi\mu\text{-}OSCPh)_4Pt]$ and $[(H_2O)Ni(\mu\text{-}OSCPh)_4Pt]$. As expected, when a bigger amount of chloride (1.5 equiv) is added to a $[(H_2O)Ni(\mu\text{-}OSCPh)_4Pt]$ solution, only the reversible peak corresponding to the $[ClNi(\mu\text{-}OSCPh)_4Pt]^-/[ClNi(\mu\text{-}OSCPh)_4Pt]$ redox system is present in the CV. Interestingly, the CV of the oxidized complex $[(H_2O)Ni(\mu\text{-}OSCPh)_4PtCl]$, **2**, in CH_2Cl_2 solution (Figure 6b), is exactly specular to that of $[(H_2O)Ni(\mu\text{-}OSCPh)_4Pt]$ in presence of 1 equiv of Cl^- anions. A one-electron reduction wave appears at Ep_c = +0.82 V, whereas two backward signals are present (Ep_{a1} = +0.94 V, Ep_{a2} = +1.13 V). Thus, coherently with the CV of the reduced species, the cathodic peak has to be attributed to the reduction of a $[ClNi(\mu\text{-}OSCPh)_4Pt]$ species, with the chloride ion bound to the Ni center. However, the X-ray structure of **2** displays a Cl^- anion coordinated to the Pt center. To rationalize this behavior, a dynamic scrambling of chloride between the Ni and Pt centers of **2** in CH_2Cl_2 solution has to be invoked. Even if complex **2** is the main species in CH_2Cl_2, it is proposed to be in equilibrium with the $[ClNi(\mu\text{-}OSCPh)_4Pt]$ species, which can be reduced more easily.

Theoretical Analysis. *Optimized Structures of the Reduced Species.* In order to understand the experimental data mentioned above, we carried out quantum chemical calculations. First, the $[ClNi(\mu\text{-}OSCPh)_4Pt]^-$ and $[Ni(\mu\text{-}OSCPh)_4PtCl]^-$ structures have been optimized (Supporting Information Figure S1). In addition, the effect of a water molecule has been modeled by calculating $[ClNi(\mu\text{-}OSCPh)_4\text{-}Pt(OH_2)]^-$ and $[(H_2O)Ni(\mu\text{-}OSCPh)_4PtCl]^-$. Comparing the theoretical and experimental structures of $[ClNi(\mu\text{-}OSCPh)_4Pt]^-$, we found overall good agreement. The short Ni···Pt distance experimentally found (2.60 Å) is slightly elongated in the calculated structure (2.70 Å). In the same manner, the Pt−S distances are slightly overestimated in our calculations (experimental Pt−S average 2.33 Å vs theoretical Pt−S average 2.43 Å). Other relevant experimental distances (see Ni−O and Ni−Cl) fully agree with calculated values. Such a good match between calculated and experimental structures, found even better for the oxidized species (*vide infra*), validates our calculations for a qualitative description of the given system.

dx.doi.org/10.1021/ic501659x | *Inorg. Chem.* 2014, 53, 10553−10562

A priori, two possible coordination sites could be expected for the chloride anion. However, for the reduced compounds, only the Ni−Cl coordination mode has been experimentally observed. Accordingly, the thermodynamic comparison between $[ClNi(\mu\text{-}OSCPh)_4Pt]$ and $[Ni(\mu\text{-}OSCPh)_4PtCl]$ shows a clear preference for coordination of chloride to Ni center (ΔG = +12.5 kcal mol^{-1}). The presence of a water molecule does not invert such tendency (ΔG = +5.2 kcal·mol^{-1}), but part of the thermodynamic reluctance of moving the chloride from Ni to the Pt appears to be partially compensated by water coordination in the optimized structure. Besides, a Pt···H−OH interaction is observed, which can be described as a hydrogen bond as previously described for other Pt(II) compounds.[31−33] It is noteworthy that the calculated Pt···Cl distances in all theoretical structures (Supporting Information Figure S1) are too large to be considered as a coordination bond distance ($d_{Pt\cdots Cl}$= 2.67 Å in $[Ni(\mu\text{-}OSCPh)_4PtCl]^-$ and $d_{Pt\cdots Cl}$= 2.71 Å in $[H_2ONi(\mu\text{-}OSCPh)_4PtCl]^-$). This is consistent with the marked preference of Pt(II) for a square planar coordination geometry over a five-coordinated geometry. Therefore, in the reduced state only the $[ClNi(\mu\text{-}OSCPh)_4Pt]^-$ structure for the $[MM'X]^-$ anion can be considered.

Optimized Structures of the Oxidized Species. In a further step of our analysis, four different structures for the oxidized [MM′X] species were explored (Supporting Information Figure S2), such as in the case of the reduced species. In that case, the preferred coordination mode for the chloride anion is Pt−Cl versus Ni−Cl, which agrees well with the experimental structure. Comparing the optimized and experimental structures of $[(H_2O)Ni(\mu\text{-}OSCPh)_4PtCl]$ we found an overall good agreement. Upon oxidation, a decrease in the Ni···Pt distance of 0.11 Å is experimentally observed. The same tendency is found in the calculated structures (0.18 Å). According to orbital analysis (*vide infra*) such effect is due to the removal of one electron from an antibonding combination of d_{z^2} orbitals of both metal centers. In the oxidized species the discrepancy between calculated and experimental Ni···Pt distances is remarkably small (0.03 Å). Differences between relevant experimental and calculated distances (Pt−Cl, Pt−S, Ni−O) are always below 0.1 Å.

Redox Properties. Having the calculated structures of the reduced and oxidized species enabled us to make a theoretical estimation of the redox potentials for each redox couple, by means of a simple thermodynamic cycle (Table 2).[34] Remarkably, for the $[ClNi(\mu\text{-}OSCPh)_4Pt(OH_2)]^-/[ClNi(\mu\text{-}OSCPh)_4Pt(OH_2)]$ couple, the value found is *ca.* 1 V versus Ag/AgCl, which is very close to the experimentally observed redox potential (0.87 V). In contrast, the calculated potentials of the other redox couples notably deviate from the experimental value. This confirms that the electrochemical behavior concerns the $[ClNi(\mu\text{-}OSCPh)_4Pt(OH_2)]^-/[Cl-Ni(\mu\text{-}OSCPh)_4Pt(OH_2)]$ couple. Interestingly, the presence of a water molecule that coordinates to the platinum center not only stabilizes the oxidized species but is also crucial to modulate the potential in such a way that the given value is lower than that for the Cl^-/Cl_2 couple. Such stabilization is even higher when $Ni-OH_2$ coordination occurs resulting in a potential of 0.2 V, which is far from the experimental value. As a consequence, the most stable oxidized species is the $[(H_2O)\text{-}Ni(\mu\text{-}OSCPh)_4PtCl]$ compound, which has been experimentally isolated. However, the reduction peak observed in the CV of the oxidized species should be attributed to the isomer $[ClNi(\mu\text{-}OSCPh)_4Pt(OH_2)]$, which implies, as discussed below, an efficient chloride scramble process.

Figure 7 shows the natural orbitals of reduced species $[ClNi(\mu\text{-}OSCPh)_4Pt(OH_2)]^-$ and $[(H_2O)Ni(\mu\text{-}_2SCPh)_4PtCl]^-$, and oxidized compounds $[ClNi(\mu\text{-}OSCPh)_4Pt(OH_2)]$ and $[(H_2O)Ni(\mu\text{-}OSCPh)_4PtCl]$. A similar scenario is observed independently on the position of chloride anion. The most stable spin state for the reduced species is always a triplet. Closed shell and open shell singlet states have been computed, but found to be at least 15 kcal mol^{-1} less stable than the

Table 2. Redox Potentials (vs Ag/AgCl) Calculated for the Oxidation of $[Cl-Ni(\mu\text{-}OSCPh)_4Pt]^-$, $[Ni(\mu\text{-}OSCPh)_4Pt\cdots Cl]^-$, $[Cl-Ni(\mu\text{-}OSCPh)_4Pt\cdots OH_2]^-$, and $[H_2O-Ni(\mu\text{-}OSCPh)_4Pt\cdots Cl]^-$

reduced species	oxidized species	oxidation potential (vs Ag/AgCl)
$[Cl-Ni(\mu\text{-}OSCPh)_4Pt]^-$	$[Cl-Ni(\mu\text{-}OSCPh)_4Pt]$	1.5 V
$[Ni(\mu\text{-}OSCPh)_4Pt\cdots Cl]^-$	$[Ni(\mu\text{-}OSCPh)_4Pt-Cl]$	1.6 V
$[Cl-Ni(\mu\text{-}OSCPh)_4Pt\cdots OH_2]^-$	$[Cl-Ni(\mu\text{-}OSCPh)_4Pt-OH_2]$	1.0 V
$[H_2O-Ni(\mu\text{-}OSCPh)_4Pt\cdots Cl]^-$	$[H_2O-Ni(\mu\text{-}OSCPh)_4Pt-Cl]$	0.2 V

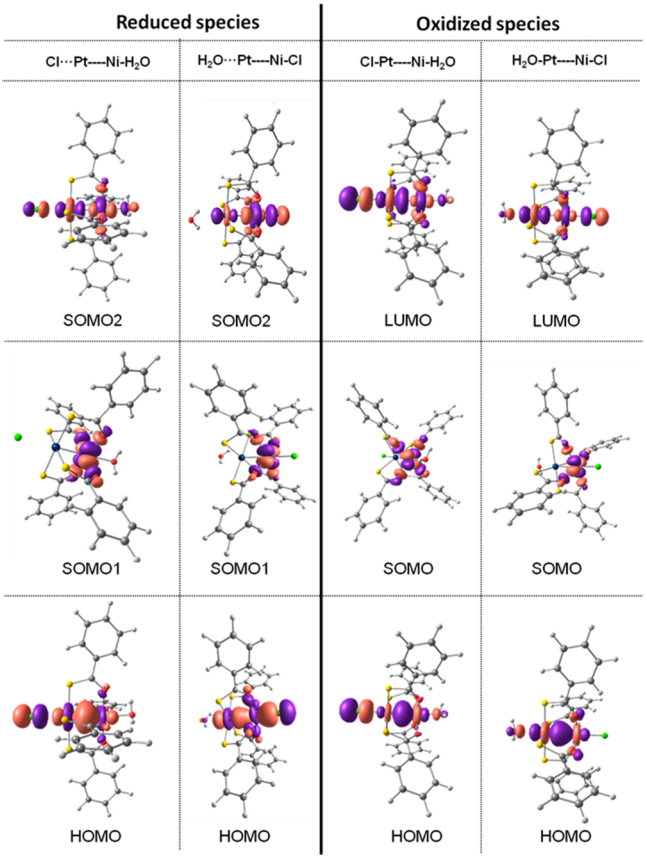

Figure 7. Representative natural orbitals for reduced ($[H_2O-Ni(\mu\text{-}OSCPh)_4Pt\cdots Cl]^-$ and $[Cl-Ni(\mu\text{-}OSCPh)_4Pt\cdots H_2O]^-$) and oxidized ($[H_2O-Ni(\mu\text{-}OSCPh)_4Pt-Cl]$ and $[Cl-Ni(\mu\text{-}OSCPh)_4Pt-H_2O]$) species.

dx.doi.org/10.1021/ic501659x | *Inorg. Chem.* 2014, 53, 10553−10562

corresponding triplet structure. Thus, for the reduced species, two different molecular orbitals contain one unpaired electron: one electron located in an essentially $d_{x^2-y^2}$ orbital in the nickel center and the second based on an antibonding d_{z^2}-d_{z^2} combination from both metal centers, with a significant contribution of p_z from the chloride anion. The same bonding combination appears as the doubly occupied orbital highest in energy. A similar orbital diagram is maintained after oxidation (Figure 7) with the removed electron always coming from the antibonding d_{z^2}-d_{z^2} combination. Consequently, the remaining unpaired electron is located at the nickel atom. This allows us to rationalize the significant decrease of Ni···Pt distance upon the oxidation process, involving a multicenter fragment. The assignment of the oxidation states of the metal ions is thus far from being obvious. Curiously, despite the unpaired electron is located at the Ni ion, it does not become a pure Ni(III) center. On the other hand, even if the oxidized product contains a chloride ligand coordinated to the platinum center, it does not mean that it is a Pt(III) ion. Supporting Information Table S1 shows the charges in reduced and oxidized species from the natural population analysis. While the absolute numbers are difficult to associate to a physical property, the difference in analogous systems gives a good idea of redistribution of electron density. In any case there is not a single atom that accommodates the major part of the positive charge induced by oxidation, which is in good agreement with the molecular orbital picture described above. The corresponding decrease of electron density is distributed between metal centers, chloride anion, and sulfur and oxygen atoms. Remarkably, oxidation of $[ClNi(\mu\text{-}OSCPh)_4Pt(OH_2)]$ or $[(H_2O)Ni(\mu\text{-}OSCPh)_4PtCl]$ results in a different electron density redistribution. First, for the $[ClNi(\mu\text{-}OSCPh)_4Pt(OH_2)]^-/[ClNi(\mu\text{-}OSCPh)_4Pt(OH_2)]$ couple, oxidation does not induce a decrease on the electronic density in the nickel atom, but a slight increase. Decrease in electronic density is assumed by other atoms, but not by nickel. On the other hand, for the couple $[(H_2O)Ni(\mu\text{-}OSCPh)_4PtCl]^-/[(H_2O)Ni(\mu\text{-}OSCPh)_4PtCl]$ the atom that supports a major degree of electron density decrease is the chloride anion.

Dynamic Chloride Exchange in Oxidized Species. From the electrochemical behavior experimentally observed, the chloride anion should easily migrate from the platinum center to the nickel center in the oxidized species. Indeed, as shown in Supporting Information Figure S3, the $[(H_2O)\cdots ClNi(\mu\text{-}OSCPh)_4PtCl]^-$ species is practically isoenergetic to $[Cl\cdots(H_2O)Ni(\mu\text{-}OSCPh)_4PtCl]$. This finding suggests as a feasible mechanism for chloride scrambling, an associative process that can be favored in the presence of an excess of chloride anions in solution. However, since only catalytic amounts of chloride are required to mediate the $[(H_2O)Ni(\mu\text{-}OSCPh)_4PtCl]/[ClNi(\mu\text{-}OSCPh)_4Pt(OH_2)]$ exchange, it can be envisaged that minor spontaneous water/chloride exchange in $[(H_2O)Ni(\mu\text{-}OSCPh)_4PtCl]$ could generate enough chlorides in the media to initiate such isomerization. Once the migration of chloride is kinetically feasible, the thermodynamics of the system is shifted by the application of an electrochemical potential leading to the oxidation of $[ClNi(\mu\text{-}OSCPh)_4Pt(OH_2)]$.

Can Polymeric Chains be Obtained? Once the oxidation of heterodimetallic NiPt units was carefully studied, the final question was whether such $[Ni(\mu\text{-}OSCPh)_4PtCl]$ fragments can be assembled to form chains or not. To answer this question we first tried experiments in solution at low temperature looking for spectroscopic evidence of supramolecular aggregation in a similar way as is observed for $[Pt_2(\mu\text{-}S_2CR)_4I]_n$.[13] However, in this case no evidence of aggregation was found. In a further effort to understand why chains are not formed from the $[Ni(\mu\text{-}OSCPh)_4Pt{-}Cl]$ fragments, we optimized the $[Ni(\mu\text{-}OSCPh)_4PtClNi(\mu\text{-}OSCPh)_4PtCl]$ aggregate and studied the possible modes of cleavage. Asymmetric cleavage should result in formation of the $[Ni(\mu\text{-}OSCPh)_4Pt]$ and $[ClNi(\mu\text{-}OSCPh)_4PtCl]$ units in a similar way as $[Pt_2(\mu\text{-}S_2CR)_4I]_n$ polymers disassemble in solution.[13] To evaluate such cleavage mode, it is enough to compare the optimized structures of $[Ni(\mu\text{-}OSCPh)_4PtClNi(\mu\text{-}OSCPh)_4PtCl]$ as a singlet or a triplet spin state. While the triplet spin state maintains the cohesion of the tetrametallic structure, the singlet spin state results in segregation of the fragments resulting from the asymmetric cleavage (Figure 8).

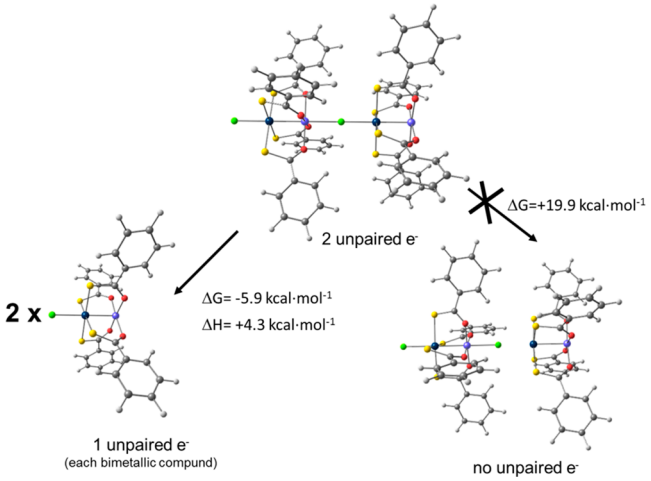

Figure 8. Thermodynamic evaluation of symmetric and asymmetric cleavage of the tetrametallic aggregate $[Ni(\mu\text{-}OSCPh)_4Pt{-}Cl{-}Ni(\mu\text{-}OSCPh)_4Pt{-}Cl]$.

Energetic difference between the triplet and singlet spin states (19.9 kcal·mol^{-1}) clearly indicates that asymmetric cleavage is energetically prohibitive. Thus, according to experimental and theoretical observations heterobimetallic NiPt MM′X chains should behave differently from diplatinum MMX chains.[7] For the symmetric cleavage a difference in enthalpy and Gibbs energy in solution between the tetrametallic aggregate and the separated bimetallic units is observed (Figure 8). In such values, basis superposition was also corrected. In terms of enthalpy, association of $[Ni(\mu\text{-}OSCPh)_4PtCl]$ fragments is slightly favorable (−4.3 kcal mol^{-1} per bimetallic compound). However, the entropic cost of assembly makes the free energy difference positive (+5.9 kcal mol^{-1}). Accordingly, no association is experimentally observed in solution at room temperature (and even at low temperature). However, since negative values of enthalpy are found, the possibility of having MM′X chains in crystal phase is not discarded. One way to obtain such linear MM′X structures is to overcome the tendency of the nickel center to coordinate a water molecule. To evaluate the interaction of water molecule with the oxidized bimetallic species, we computed the thermodynamics of the interaction in solution between water and the fragment $[Ni(\mu\text{-}OSCPh)_4PtCl]$, taking into account the basis superposition correction. For coordination of water to nickel, the enthalpy of interaction is markedly favorable (−12.3 kcal mol^{-1}). Entropic

dx.doi.org/10.1021/ic501659x | Inorg. Chem. 2014, 53, 10553−10562

cost in this case does not change the sign of Gibbs energy in solution (−2.9 kcal mol^{-1}), with coordination of water being slightly favorable at room temperature in solution, which is in good agreement with experimental observations.

CONCLUSIONS

Oxidation of Ni···Pt bimetallic species [Ni(μ-OSCPh)$_4$Pt] is only possible when assisted by coordination of both chloride anion and water molecule, since these ligands increase the overall electronic density. Thus, it has been found that, from the stable reduced species (PNP)[ClNi(μ-OSCPh)$_4$Pt], the also stable [(H$_2$O)Ni(μ-OSCPh)$_4$PtCl] oxidized species can be obtained. According to experimental electrochemical data a NiPt−Cl/Cl−NiPt isomerization process is available in the oxidized species but not in its reduced state. In good agreement, calculations suggest for such exchange an associative mechanism. Theoretical examination of electronic structure shows a rather uncommon scenario, which can be understood as a combination of d^8 square planar orbital diagram for Pt(II) and d^8 octahedral orbital diagram for the Ni(II) center. Thus, the reduced state contains two unpaired electrons, one located in an essentially $d_{x^2-y^2}$ orbital in the Ni(II) and the other in the antibonding d_{z^2}-d_{z^2} combination from Ni(II) and Pt(II) centers, in agreement with magnetic susceptibility, with a remarkable contribution of p_z from chloride anion. When oxidation occurs, it is from this second molecular orbital that the electron is removed, also in agreement with magnetic susceptibility and EPR measurements. As a consequence, while the unpaired electron in the oxidized species is located mainly in the nickel atom, the oxidation process occurred not in a single atom but in a multicenter fragment. The possibility to isolate MM′X chains is restricted by the high tendency of Ni centers in the oxidized species to coordinate slightly coordinating solvents such as water and thus quench the chain growth. Consequently, further efforts for obtaining heterometallic PtNiX polymers should be addressed by trying to remove water molecules from the dimetal complexes. However, this should be done after the oxidation process because H$_2$O is required to decrease the oxidation potential of the reduced species.

EXPERIMENTAL SECTION

Materials and Methods. [(H$_2$O)Ni(μ-OSCPh)$_4$Pt][6] and iodobenzene dichloride[35] were prepared according to reported procedures. All other reagents and solvents were used as received. ^{1}H NMR spectra were recorded on a on a Bruker AMX-300 spectrometer using standard Bruker pulse sequences. Chemical shifts are reported in ppm referenced to residual solvent protons (CD_2Cl_2). FTIR spectra (KBr pellets) were recorded on a PerkinElmer 1650 spectrophotometer. Electronic absorption spectra were recorded on an Agilent 8452 diode array spectrophotometer over a range λ = 190−1100 nm in 0.2 and 1 cm quartz cuvettes. C, H, N, S elemental analyses were performed on a Perkin−Elmer 240-B microanalyzer. Electrospray mass (ESI-MS) spectra were recorded on a QSTAR Pulsar mass spectrometer from Applied Biosystems, equipped with a hybrid analyzer Q-TOF (quadrupole time-of-flight). The samples were analyzed in positive and negative ionization mode by direct perfusion in the ESI source, using a syringe pump at a flow rate of 20 μL/min (ion spray voltage, +5550 V for positive ionization mode and −4500 V for negative ionization mode; focusing potential, ±210 V; declustering potential, ±30 V; declustering potential 2, ±15 V). The thermogravimetric analyses were performed in a TGA TA INSTRUMENTS Q-500 analyzer. The temperature program was from 25 to 1000 °C, with a temperature rate 5 °C min^{-1} under a nitrogen flow.

*Synthesis of (PPN)[ClNi(μ-OSCPh)$_4$Pt] (**1**).* Solid bis(triphenylphosphoranylidene)ammonium chloride (0.072 g, 0.122 mmol) was added to a solution of [(H$_2$O)Ni(μ-OSCPh)$_4$Pt] (20.0 mg, 0.024 mmol) in CH_2Cl_2 (5 mL). X-ray suitable yellow single crystals of [**1**]·0.5CH_2Cl_2 were obtained by layering pentane into this solution at 20 °C. The product was filtered, washed with pentane, and dried (0.025 g, 0.018 mmol, 73%). IR (cm^{-1}): 3435w br, 3052w, 2974w, 2927w, 2880w, 1540w, 1508s, 1495s, 1482m, 1436m, 1304w, 1213s, 1171s, 1114w, 950w, 774s, 746w, 723m, 708m, 689m, 645w, 544w Anal. Calcd for $C_{64}H_{50}ClNNiO_4P_2PtS_4$·$CH_2Cl_2$ (1418.98): C, 53.27; H, 3.85; N, 0.96; S, 8.75. Found: C, 53.62; H, 3.80; N, 1.00; S, 8.77.

*Synthesis of [(H$_2$O)Ni(μ-OSCPh)$_4$PtCl] (**2**).* Solid iodobenzene dichloride (0.052 g, 0.19 mmol) was added to a solution of [(H$_2$O)Ni(μ-OSCPh)$_4$Pt] (0.265 g, 0.323 mmol) in THF (20 mL) at 20 °C, with color change from light yellow to dark purple. After 1 h, pentane (20 mL) was added to the reaction vessel, with consequent formation of a dark purple precipitate. The precipitation was completed by cooling the mixture at −18 °C for 2 h. The dark purple microcrystalline powder was filtered, washed with pentane (10 mL), and dried in vacuum (**2**·THF, 0.175 g, 0.189 mmol, 58%). IR (cm^{-1}): 3425w br, 3057w, 2975w, 2925w, 2888w, 2853w, 1594w, 1535s, 1495s, 1485m, 1445m, 1306w, 1218s, 1173s, 1034w, 1000w, 955s, 881w, 770m, 715m, 686m, 647w, 582w. ^{1}H NMR (300 MHz, CD_2Cl_2): δ ∼12.30 (s br), 8.33 (s), 7.46 (s), ∼1.51 (s br). ESI-MS (CH_2Cl_2, negative ionization mode, m/z, I%): 734.9, 100 [PtNi(PhCOS)$_3$Cl$_2$]$^-$; 871.8, 70 [PtNi(PhCOS)$_4$Cl$_2$]$^-$; 949.8, 40 [PtNi(PhCOS)$_4$Cl$_2$·DMSO]$^-$; 1710.6, 40 [(PtNi(PhCOS)$_4$)$_2$Cl$_3$]$^-$. Anal. Calcd for $C_{28}H_{22}ClNiO_5PtS_4$·C_4H_8O (928.07): C, 41.41; H, 3.26; N, 0.00; S, 13.82. Found: C, 41.71; H, 3.24; N, 0.02; S, 13.90. X-ray suitable single crystals of **2**·2THF were obtained by layering pentane onto a THF solution of the product at −18 °C.

Electrochemistry. Cyclic voltammetry experiments were performed under an argon atmosphere at room temperature in CH_2Cl_2 solutions. Tetrabutylammonium hexafluorophosphate (Bu_4NPF_6) was used as supporting electrolytes. Measurements were carried out by using an Ivium CompaqStat potentiostat interfaced with a computer. A standard three-electrode electrochemical cell was used. Potentials were referred to an Ag/AgCl, Et$_4$NBr 0.4 M reference electrode in ethylene glycol, and measured potentials were calibrated through the use of an internal Fc/Fc$^+$ standard. The working electrode was a vitreous carbon disk (3 mm in diameter), previously polished with alumine powder or by sonication (Ep_a, anodic peak potential; Ep_c, cathodic peak potential; $E_{1/2} = (Ep_a + Ep_c)/2$; $\Delta E_p = Ep_a - Ep_c$). The auxiliary electrode was a Pt wire.

X-ray Diffraction Data Collection and Structure Determination. The X-ray diffraction data collections and structure determinations were done on a Bruker SMART 6K CCD diffractometer with graphite-monochromated Mo Kα radiation (λ = 0.710 73 Å). All the structures were solved by direct methods using the SIR92 program[36] and refined by full-matrix least-squares on F^2 including all reflections (SHELXL97).[37] All calculations were performed using the WINGX crystallographic software package.[38] The crystal structure of compound **2** showed the presence of disordered dichloromethane and water solvation molecules that were refined with half occupation factors. Soft restraints were applied to impose C−Cl bond distances to be similar in both dichloromethane disordered molecules. The hydrogen atoms of the disordered water molecule were not located. Crystal parameters and details of the final refinements of compounds **1** and **2** are summarized in Table 3.

EPR Spectroscopy. X-band EPR spectra were recorded on a Bruker EMX spectrometer, equipped with the ER-4192 ST Bruker cavity and an ER-4131 VT at 100 K.

Magnetic Measurements. The magnetic susceptibility measurements were carried out in the temperature range 2−300 K with an applied magnetic field of 0.5 T on polycrystalline samples of compounds **1** and **2** (with masses of 8.96 and 17.97 mg, respectively) with a Quantum Design MPMS-XL-5 SQUID susceptometer. The susceptibility data were corrected for the sample holders previously measured using the same conditions and for the diamagnetic contributions of the salt as deduced by using Pascal's constant tables

dx.doi.org/10.1021/ic501659x | Inorg. Chem. 2014, 53, 10553−10562

Table 3. Crystallographic Data and Structure Refinement Details of compounds 1 and 2

	1	2
empirical formula	$C_{65}H_{53}Cl_3NNiO_{4.5}P_2PtS_4$	$C_{36}H_{38}ClNiO_7PtS_4$
fw	1470.41	1000.15
λ (Å)	0.710 73	0.710 73
T (K)	296(2)	100(2)
cryst syst	triclinic	orthorhombic
space group	$P\bar{1}$	$Pna2_1$
a (Å)	13.6987(3)	21.743(5)
b (Å)	15.2734(3)	11.782(2)
c (Å)	16.4063(4)	14.893(3)
α (deg)	93.783(1)	90
β (deg)	104.633(1)	90
γ (deg)	106.144(1)	90
V (Å^3)	3155.85(12)	3815.2(13)
Z	2	4
ρ_{calcd} (g cm^{-3})	1.547	1.741
μ (mm^{-1})	2.871	4.492
reflns collected	47 332	20 057
unique data/params	11 524/731	6736/451
R_{int}	0.0462	0.1226
GOF (S)[a]	1.073	0.998
R1[b]/wR2[c] [$I > 2\sigma(I)$]	0.0452/0.1225	0.0554/0.1214
R1[b]/wR2[c] (all data)	0.0773/0.1511	0.1321/0.2183

[a] $S = [\sum w(F_o^2 - F_c^2)^2/(N_{obs} - N_{param})]^{1/2}$. [b] $R1 = \sum||F_o| - |F_c||/\sum|F_o|$. [c] $wR2 = [\sum w(F_o^2 - F_c^2)^2/\sum wF_o^2]^{1/2}$; $w = 1/[\sigma^2(F_o^2) + (aP)^2 + bP]$ where $P = (\max(F_o^2,0) + 2F_c^2)/3$ with $a = 0.0859$ (1), 0.1012 (2), and $b = 0.5238$ (1).

(χ_{dia}= −805 × 10^{-6} and −493 × 10^{-6} cm^3 mol^{-1} for 1 and 2, respectively).[39]

DFT Calculations. All calculations were carried out at the DFT level, using the M06 functional[40−42] with an ultrafine Grid[43] implemented in Gaussian09.[44] The C and H atoms were described with the 6-31G(d,p) basis set while for O, Cl, and S atoms 6-31G+(d) was used.[45,46] However, Pt and Ni were described using an effective core potential SDD for the inner electron and its associated double-ζ basis set for the outer ones,[47] complemented with a set of f-polarization functions.[48] Harmonic frequencies were computed analytically to classify the stationary points as minima. These calculations were also used to determine the difference between the Gibbs and potential energies in gas phase (Ggp − Egp), which includes the zero-point, thermal, and entropy corrections. The effect of the dichloromethane solvent (ε = 8.93) was estimated by computing the energy in solvent (EDCM) by means of single-point calculations on gas-phase optimized geometries with the solvation model density (SMD) continuum solvation model.[49] All the energies given in the text are Gibbs energies in solution, GDCM, which were calculated by adding thermal and entropic corrections to the SMD energies.

■ ASSOCIATED CONTENT

Supporting Information

Additional figures, a table of the charge distribution from natural population analysis, coordinates of the calculated structures, and crystallographic data in CIF format for compounds 1 and 2. This material is available free of charge via the Internet at http://pubs.acs.org.

■ AUTHOR INFORMATION

Corresponding Authors

*E-mail: ruben.mas@uam.es.

*E-mail: felix.zamora@uam.es.

Author Contributions

The manuscript was written through contributions of all authors. All authors have given approval to the final version of the manuscript.

Notes

The authors declare no competing financial interest.

■ ACKNOWLEDGMENTS

This research was financially supported by the Spanish MINECO (MAT2013-46753-C2-1-P and CTQ2011-26507), the Comunidad de Madrid (CAM 09-S2009_MAT-1467), and the Generalidad Valenciana (Prometeo and ISIC projects).

■ REFERENCES

(1) Batten, S. R.; Neville, S. M.; Turner, D. *Coordination Polymers: Design, Analysis and Applications*; RSC Publishing: London, 2009; Vol. 7.

(2) Cotton, F. A.; Murillo, C. A.; Walton, R. A. *Multiple Bonds Between Metal Atoms*, 3rd Ed.; Springer Science and Business Media Inc.: New York, 2005.

(3) Bera, J. K.; Dunbar, K. R. *Angew. Chem., Int. Ed.* **2002**, *41*, 4453−4457.

(4) Cotton, F. A.; Lin, C.; Murillo, C. A. *Acc. Chem. Res.* **2001**, *34*, 759−771.

(5) Baddour, F. G.; Fiedler, S. R.; Shores, M. P.; Bacon, J. W.; Golen, J. A.; Rheingold, A. L.; Doerrer, L. H. *Inorg. Chem.* **2013**, *52*, 13562−13575.

(6) Dahl, E. W.; Baddour, F. G.; Fiedler, S. R.; Hoffert, W. A.; Shores, M. P.; Yee, G. T.; Djukic, J. P.; Bacon, J. W.; Rheingold, A. L.; Doerrer, L. H. *Chem. Sci.* **2012**, *3*, 602−609.

(7) Givaja, G.; Castillo, O.; Mateo, E.; Gallego, A.; Gomez-Garcia, C. J.; Calzolari, A.; di Felice, R.; Zamora, F. *Chem.—Eur. J.* **2012**, *18*, 15476−15484.

(8) Yamashita, M.; Okamoto, H. e. *Material Designs and New Physical Properties in MX- and MMX-Chain Compounds*; Springer-Verlag: Vienna, 2013.

(9) Mas-Balleste, R.; Gomez-Herrero, J.; Zamora, F. *Chem. Soc. Rev.* **2010**, *39*, 4220−4233.

(10) Kitagawa, H.; Onodera, N.; Sonoyama, T.; Yamamoto, M.; Fukawa, T.; Mitani, T.; Seto, M.; Maeda, Y. *J. Am. Chem. Soc.* **1999**, *121*, 10068−10080.

(11) Mitsumi, M.; Murase, T.; Kishida, H.; Yoshinari, T.; Ozawa, Y.; Toriumi, K.; Sonoyama, T.; Kitagawa, H.; Mitani, T. *J. Am. Chem. Soc.* **2001**, *123*, 11179−11192.

(12) Gentili, D.; Givaja, G.; Mas-Balleste, R.; Azani, M. R.; Shehu, A.; Leonardi, F.; Mateo-Marti, E.; Greco, P.; Zamora, F.; Cavallini, M. *Chem. Sci.* **2012**, *3*, 2047−2051.

(13) Azani, M. R.; Paz, A. P.; Hermosa, C.; Givaja, G.; Gomez-Herrero, J.; Mas-Balleste, R.; Zamora, F.; Rubio, A. *Chem.—Eur. J.* **2013**, *19*, 15518−15529.

(14) Welte, L.; García-Couceiro, U.; Castillo, O.; Olea, D.; Polop, C.; Guijarro, A.; Luque, A.; Gómez-Rodríguez, J. M.; Gómez-Herrero, J.; Zamora, F. *Adv. Mater.* **2009**, *21*, 2025−2028.

(15) Welte, L.; Calzolari, A.; di Felice, R.; Zamora, F.; Gómez-Herrero, J. *Nat. Nanotechnol.* **2010**, *5*, 110−115.

(16) Hermosa, C.; Alvarez, J. V.; Azani, M. R.; Gomez-Garcia, C. J.; Fritz, M.; Soler, J. M.; Gomez-Herrero, J.; Gomez-Navarro, C.; Zamora, F. *Nat. Commun.* **2013**, *4*, 1709.

(17) Gomez-Herrero, J.; Zamora, F. *Adv. Mater.* **2011**, *23*, 5311−5317.

(18) Jimenez-Aparicio, R.; Urbanos, F. A.; Arrieta, J. M. *Inorg. Chem.* **2001**, *40*, 613−619.

(19) Barral, M. C.; Jimenez-Aparicio, R.; Priego, J. L.; Royer, E. C.; Urbanos, F. A.; Amador, U. *Inorg. Chem.* **1998**, *37*, 1413−1420.

(20) Olea, D.; Gonzalez-Prieto, R.; Priego, J. L.; Barral, M. C.; de Pablo, P. J.; Torres, M. R.; Gomez-Herrero, J.; Jimenez-Aparicio, R.; Zamora, F. *Chem. Commun.* **2007**, 1591−1593.

(21) Kuwahara, R.; Fujikawa, S.; Kuroiwa, K.; Kimizuka, N. *J. Am. Chem. Soc.* **2012**, *134*, 1192−1199.
(22) Demadis, K. D.; Hartshorn, C. M.; Meyer, T. J. *Chem. Rev.* **2001**, *101*, 2655−2685.
(23) Mitsumi, M.; Kitamura, K.; Morinaga, A.; Ozawa, Y.; Kobayashi, M.; Toriumi, K.; Iso, Y.; Kitagawa, H.; Mitani, T. *Angew. Chem., Int. Ed.* **2002**, *41*, 2767−2771.
(24) Bellitto, C.; Flamini, A.; Gastaldi, L.; Scaramuzza, L. *Inorg. Chem.* **1983**, *22*, 444−449.
(25) Mitsumi, M.; Yoshida, Y.; Kohyama, A.; Kitagawa, Y.; Ozawa, Y.; Kobayashi, M.; Toriumi, K.; Tadokoro, M.; Ikeda, N.; Okumura, M.; Kurmoo, M. *Inorg. Chem.* **2009**, *48*, 6680−6691.
(26) Guijarro, A.; Castillo, O.; Welte, L.; Calzolari, A.; Miguel, P. J. S.; Gomez-Garcia, C. J.; Olea, D.; di Felice, R.; Gomez-Herrero, J.; Zamora, F. *Adv. Funct. Mater.* **2010**, *20*, 1451−1457.
(27) Uemura, K.; Fukui, K.; Yamasaki, K.; Matsumoto, K.; Ebihara, M. *Inorg. Chem.* **2010**, *49*, 7323−7330.
(28) Uemura, K.; Yamasaki, K.; Fukui, K.; Matsumoto, K. *Eur. J. Inorg. Chem.* **2007**, 809−815.
(29) Kahn, O. In *Molecular Magnetism*; VCH Publishers: New York, 1993.
(30) Ginsberg, A. P.; Brookes, R. W.; Martin, R. L.; Sherwood, R. C. *Inorg. Chem.* **1972**, *11*, 2884−2892.
(31) Berges, J.; Fourre, I.; Pilme, J.; Kozelka, J. *Inorg. Chem.* **2013**, *52*, 1217−1227.
(32) Rizzato, S.; Berges, J.; Mason, S. A.; Albinati, A.; Kozelka, J. *Angew. Chem., Int. Ed.* **2010**, *49*, 7440−7443.
(33) Vidossich, P.; Ortuno, M. A.; Ujaque, G.; Lledos, A. *ChemPhysChem* **2011**, *12*, 1666−1668.
(34) Konezny, S. J.; Doherty, M. D.; Luca, O. R.; Crabtree, R. H.; Soloveichik, G. L.; Batista, V. S. *J. Phys. Chem. C* **2012**, *116*, 6349−6356.
(35) Powers, D. C.; Benitez, D.; Tkatchouk, E.; Goddard, W. A.; Ritter, T. *J. Am. Chem. Soc.* **2010**, *132*, 14092−14103.
(36) Ferey, G. *Dalton Trans.* **2009**, 4400−4415.
(37) Tanh Jeazet, H. B.; Staudt, C.; Janiak, C. *Dalton Trans.* **2012**, *41*, 14003−14027.
(38) Prakash, M. J.; Lah, M. S. *Chem. Commun.* **2009**, 3326−3341.
(39) Bain, G. A.; Berry, J. F. *J. Chem. Educ.* **2008**, *85*, 532−536.
(40) Reed, A. E.; Weinstock, R. B.; Weinhold, F. *J. Chem. Phys.* **1985**, *83*, 735−746.
(41) Bader, R. F. W. *Atoms in Molecules. A Quantum Theory*; Clarendon Press: Oxford, 1990.
(42) Keith, T. A. TK Gristmill Software: Overland Park, KS, 2014 (aim.tkgristmill.com).
(43) Wheeler, S. E.; Houk, K. N. *J. Chem. Theory Comput.* **2010**, *6*, 395−404.
(44) Frisch, M. J.; Trucks, G. W.; Schlegel, H. B.; Scuseria, G. E.; Robb, M. A.; Cheeseman, J. R.; Scalmani, G.; Barone, V.; Mennucci, B.; Petersson, G. A.; Nakatsuji, H.; Caricato, M.; Li, X.; Hratchian, H. P.; Izmaylov, A. F.; Bloino, J.; Zheng, G.; Sonnenberg, J. L.; Hada, M.; Ehara, M.; Toyota, K.; Fukuda, R.; Hasegawa, J.; Ishida, M.; Nakajima, T.; Honda, Y.; Kitao, O.; Nakai, H.; Vreven, T.; Montgomery, J. A., Jr.; Peralta, J. E.; Ogliaro, F.; Bearpark, M.; Heyd, J. J.; Brothers, E.; Kudin, K. N.; Staroverov, V. N.; Kobayashi, R.; Normand, J.; Raghavachari, K.; Rendell, A.; Burant, J. C.; Iyengar, S. S.; Tomasi, J.; Cossi, M.; Rega, N.; Millam, N. J.; Klene, M.; Knox, J. E.; Cross, J. B.; Bakken, V.; Adamo, C.; Jaramillo, J.; Gomperts, R.; Stratmann, R. E.; Yazyev, O.; Austin, A. J.; Cammi, R.; Pomelli, C.; Ochterski, J. W.; Martin, R. L.; Morokuma, K.; Zakrzewski, V. G.; Voth, G. A.; Salvador, P.; Dannenberg, J. J.; Dapprich, S.; Daniels, A. D.; Farkas, Ö.; Foresman, J. B.; Ortiz, J. V.; Cioslowski, J.; Fox, D. J. *Gaussian 09, Revision A.1*; Gaussian, Inc.: Wallingford, CT, 2009.
(45) Hehre, W. J.; Ditchfie, R.; Pople, J. A. *J. Chem. Phys.* **1972**, *56*, 2257−2264.
(46) Francl, M. M.; Pietro, W. J.; Hehre, W. J.; Binkley, J. S.; Gordon, M. S.; Defrees, D. J.; Pople, J. A. *J. Chem. Phys.* **1982**, *77*, 3654−3665.
(47) Andrae, D.; Haussermann, U.; Dolg, M.; Stoll, H.; Preuss, H. *Theor. Chim. Acta* **1990**, *77*, 123−144.
(48) Ehlers, A. W.; Bohme, M.; Dapprich, S.; Gobbi, A.; Hollwarth, A.; Jonas, V.; Kohler, K. F.; Stegmann, R.; Veldkamp, A.; Frenking, G. *Chem. Phys. Lett.* **1993**, *208*, 111−114.
(49) Marenich, A. V.; Cramer, C. J.; Truhlar, D. G. *J. Phys. Chem. B* **2009**, *113*, 6378−6396.